DOI: 10.1002/chem.200701946

Three-Dimensional Mesoporous Gallosilicate with *Pm3n* Symmetry and its Unusual Catalytic Performances

Pavuluri Srinivasu and Ajayan Vinu*[a]

Abstract: Three-dimensional, mesoporous-cage-type, GaSBA-1 materials with different n_{Si}/n_{Ga} ratios have been successfully prepared for the first time by using a low hydrochloric acid to silicon (n_{HCl}/n_{Si}) molar ratio in the synthesis gel by templating with cetyltriethylammonium bromide as the structure-directing agent in a highly acidic medium. The obtained materials have been unambiguously characterized in detail by several sophisticated techniques including X-ray diffraction (XRD), N_2 adsorption, high-resolution transmission electron microscopy, high-resolution scanning electron microscopy, energy dispersive spectroscopy, elemental mapping, and ^{29}Si magic-angle-spinning NMR spectroscopy. XRD and nitrogen adsorption results reveal that the structures of the GaSBA-1 materials resemble that of SBA-1, which possesses a cubic, three-dimensional, cage-type structure with open windows. In addition, the specific surface area and the specific pore volume of the GaSBA-1 materials are much higher than those of the SBA-1 silica, which are very important for the catalytic applications. The amount of Ga cation in the SBA-1 silica framework has been found to play a critical role in controlling the morphology and the pore diameter of the materials. Finally, the catalytic activity in the *tert*-butylation of phenol with *tert*-butanol as the alkylating agent has been investigated and the results are compared with those of other mesoporous catalysts such as AlMCM-41, FeMCM-41, FeAl-MCM-41, and FeSBA-1. Moreover, the effect of various reaction parameters such as the reaction temperature, reactant feed ratio, and time-on-stream on the phenol conversion in the *tert*-butylation of phenol over GaSBA-1 catalysts has been demonstrated. Among the catalysts examined, GaSBA-1(17), in which the number in the parenthesis denotes the n_{Si}/n_{Ga} ratio, showed remarkable activity with a high conversion of phenol and selectivity to 4-*tert*-butylphenol; it was found to be superior over other mesoporous catalysts used in the study.

Keywords: alkylation · heterogeneous catalysis · mesoporous materials · SBA-1 · scanning probe microscopy

Introduction

Mesoporous inorganic oxide materials with well-ordered porous structures are highly attractive and have received considerable attention in the recent years, because of their excellent textural parameters, such as high surface area, pore volume, and narrow pore size distribution, and potential applications mainly in the fields of catalysis, adsorption, and separation.[1–15] A variety of mesoporous inorganic oxide materials with different pore structures have been synthesized by self-assembly process under basic or acidic or neutral conditions by using cationic, anionic, or non-ionic surfactants, which are so-called structure-directing agents.[1–6,16–20] One of the interesting features of the self-assembly-mediated synthesis process is the easy control of the textural parameter and pore structure of mesoporous materials; this control is achieved by altering the type of the surfactants and co-solvents used in the reactant mixture and preparative conditions. There are numerous reports that deal with the preparation of various types of one- and three-dimensional mesoporous materials, such as MCM-41, MCM-48, SBA-1, SBA-15, AMS, HMS, and so forth.[1–20] Among these materials, mesoporous silica materials consisting of three-dimensional porous networks are highly interesting and believed to be more advantageous than the materials that have uni-dimensional array of pores. This could be mainly due to the fact that materials with three-dimensional

[a] Dr. P. Srinivasu, Dr. A. Vinu
International Center for Materials Nanoarchitectonics
World Premier International (WPI) Research Center
National Institute for Materials Science
1-1 Namiki, Tsukuba, 305-0044 (Japan)
Fax: (+81) 29-860-4563
E-mail: vinu.ajayan@nims.go.jp

Supporting information for this article is available on the WWW under http://www.chemeurj.org/ or from the author.

pore structures are more resistant to pore blocking, mass transfer of the reactant molecules in the pore channels, and provide more adsorption sites, generated from their higher surface area and pore volume, and can be easily accessible through three-dimensional pore channels for the reactant molecules.[21]

The structural features of three-dimensional, cage-type, mesoporous materials resemble very much the structures of zeolites with super cages,[3,4,18] though the cage diameter of the former is much bigger than that of the latter. These interesting textural properties make them promising candidates for shape-selective catalysis, reactions involving bulky molecules with different molecular dimensions, and adsorption experiments with differently sized hydrocarbons.[22,23] Among mesoporous materials with a cage-type pore structure, SBA-1 is the most interesting material and was discovered by Huo et al.[18] Their pore structure was elucidated by electron crystallography and HRTEM by Kruk et al.[24] Moreover, the SBA-1 material possesses a three-dimensional structure with open windows and two kinds of cage-type porous structure, the larger one has the diameter of about 4.0 nm and the diameter of the smaller cage is 3.3 nm, with excellent symmetry.[25] Moreover, the specific surface area of SBA-1 is much higher than that of the three-dimensional SBA-16 and MCM-48 materials.[3,4,18] The silica form of mesoporous SBA-1 was prepared under acidic conditions by using cationic surfactants as the structure-directing agents at low temperature; they were formed by the cooperative self-assembly mechanism, which involves the ($S^+X^-I^+$) pathway (cationic surfactants (S^+), halogen anions (X^-) and cationic silicic acid species (I^+)).[4,18,24–26]

Although the pure silica SBA-1 materials possess interesting structural features and high symmetry, their neutral framework and poor water stability make them useless for many applications, including catalysis and adsorption. These problems can be circumvented by introducing di- or trivalent heteroatoms in the neutral silica framework. The introduction of heteroatoms in the silica framework can create negative charges in the framework, which are compensated by the protons, the so-called Brønsted acid sites that are vital for acid-catalyzed transformations. However, unfortunately, it is very difficult to incorporate the metal atoms in the mesoporous materials prepared under highly acidic conditions, because the solubility of the metal source is high under such conditions. In addition, the heteroatoms exist only in the cationic forms rather than their corresponding oxo species in acidic conditions; this suppresses the contact between the heteroatoms and the silica species. Tatsumi et al. have successfully reported the synthesis of V- and Mo-containing SBA-1 by choosing the appropriate metal sources, and gained control of the crystal morphology.[27–29]

Recently, Vinu et al. have reported the direct synthesis of Al, Fe, and TiSBA-1 with different contents of metal in the framework by applying a novel synthesis approach that involves the "control of the hydrochloric acid to silicon molar ratio" in the synthesis mixture in order to enhance the interaction between the heteroatoms and the silicon species in highly acidic medium.[21,30,31] Further, they found that the above materials show excellent activity in both the acid-catalyzed transformations, especially for alkylation, acylation, isomerization, and oxidation of bulky organic molecules. Recently, gallium-substituted mesoporous materials have received much attention, because they exhibit some interesting properties and show excellent performances in many acid-catalyzed reactions.[32,33] In addition, they provide different distribution of acid site strength, which is critical for several acid-catalyzed reactions. However, unfortunately, there has been no report available on the preparation and catalytic performances of gallium-substituted SBA-1 materials in the open literature so far. Here we extend our unique synthetic strategy for the fabrication of GaSBA-1, which was previously used for the synthesis of Fe, Al, and Ti-SBA-1, in which the hydrochloric acid to silicon molar ratio in the synthesis gel is controlled to increase the metal ion incorporation in the silica matrix of SBA-1.

Alkylation and acylation of aromatics have received enormous attention in recent years because of the importance of the alkylated or acylated aromatic products that are being used as intermediates for the manufacture of antioxidants, ultraviolet absorbers, and polymerization inhibitors.[34] One of the interesting alkylated aromatics is 4-*tert*-butylphenol (4-TBP), which plays a critical role in the manufacture of lubricating oils and can be easily obtained through a simple *tert*-butylation of phenol, a process that involves the use of homogeneous catalysts such as aluminum chloride, phosphoric acid, sulphuric acid, silica-alumina, and cation exchange resins.[35] Although the reaction has been extensively studied by using homogenous catalytic systems, these catalysts pose several problems such as toxicity, corrosiveness, and other hurdles in the commercialization of the process due to the tedious steps involved in their separation from the reaction mixture. Consequently, researchers have looked for alternatives, for example, heterogeneous catalysts, such as zeolites,[36] zeotypes, and mesoporous materials, which are environmentally friendly and can avoid the problems mainly in the separation process. Recently, Selvam and co-workers reported the *tert*-butylation of phenol over monometal-substituted AlMCM-41 or FeMCM-41 and proposed that the activity and selectivity of the catalysts depend upon the nature of acid sites present. It has been also reported that the formation of 4-TBP requires catalysts with moderate acid strength.[37]

In this manuscript, we report on the preparation of the Ga-substituted SBA-1 with different loading of Ga by the simple adjustment of the hydrochloric acid to silicon (n_{HCl}/n_{Si}) molar ratio[30,31] of the synthesis gel by a templation method with cetyltriethylammonium bromide (CTEABr) as the structure-directing agent and Ga nitrate as the Ga source. The obtained materials have been thoroughly characterized by various sophisticated techniques such as X-ray diffraction (XRD), N_2 adsorption, high-resolution transmission electron microscopy (HRTEM), high-resolution scanning electron microscopy (HRSEM), energy dispersive spectroscopy (EDS), elemental mapping, and ^{29}Si magic-angle-

spinning (MAS) NMR spectroscopy. The XRD, N_2 adsorption, and HRTEM analysis showed that the structural order of the materials is retained even after the incorporation of Ga in the silica framework of SBA-1. The catalytic activity of the GaSBA-1 materials with different Ga content has been investigated on the *tert*-butylation of phenol with *tert*-butanol (TBA) as the alkylating agent; the results are compared with those of other catalysts such as FeMCM-41, AlMCM-41, FeAl-MCM-41, and FeSBA-1. Among the catalysts studied, the GaSBA-1 with the highest Ga content registers very high phenol conversion and excellent selectivity towards the 4-*tert*-butylphenol (4-TBP).

Results and Discussion

The synthesis conditions and the elemental composition of the calcined GaSBA-1 samples are given in Table 1. It can be seen that the n_{Si}/n_{Ga} ratio of the calcined GaSBA-1 samples decreases with increasing the addition of Ga source in the synthesis mixture. However, the n_{Si}/n_{Ga} ratio of the final product is higher than that added in the synthesis gel. This could be mainly due to the higher solubility of the Ga source in the highly acidic medium, which minimizes the contact between the Ga and Si–oxo species present in the synthesis mixture. Figure 1 shows the EDX pattern of the calcined GaSBA-1 samples with different n_{Si}/n_{Ga} ratios. All the samples exhibit peaks for Ga, Si, and O, confirming that the samples are mainly composed of these elements; impurities, such as Cl or C, which may be expected from the hydrochloric acid and the template, respectively, added in the synthesis gel are not found in the samples after calcination. It is interesting to note that the intensity of the Ga peak increases with the concomitant increase of the intensity of the Si peak in the EDX pattern, with increasing the amount of Ga source in the synthesis mixture. Moreover, the n_{Si}/n_{Ga} ratios obtained from the EDS patterns are consistent with the n_{Si}/n_{Ga} ratio obtained from the ICP elemental analysis. The data obtained from the ICP and EDX analyses in combination with the elemental mapping clearly confirm that Ga in SBA-1 is homogeneously distributed throughout the samples (Figure 2). Elemental mapping of the samples also reveal that the density of the Ga atom on the surface of the GaSBA-1 catalysts significantly increases when the n_{Si}/n_{Ga} ratio in the synthesis gel is decreased.

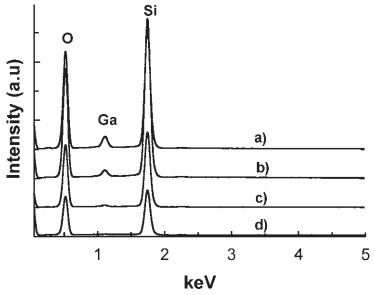

Figure 1. EDS patterns of GaSBA-1 materials with different Ga content: a) GaSBA-1(17), b) GaSBA-1(40), c) GaSBA-1(90), and d) GaSBA-1-(140).

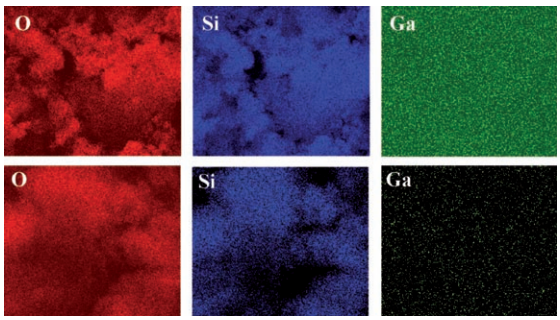

Figure 2. Elemental mapping of GaSBA-1(17) (top) and GaSBA-1(140) (bottom).

Figure 3 shows the powder XRD patterns of as-synthesized GaSBA-1 samples with different Ga contents. All the

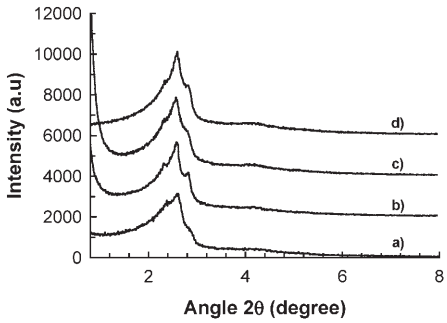

Figure 3. Powder XRD patterns of as-synthesized GaSBA-1 materials with different Ga content: a) GaSBA-1(17), b) GaSBA-1(40), c) GaSBA-1(90), and d) GaSBA-1(140).

Table 1. Textural parameters of calcined GaSBA-1 samples with different n_{Si}/n_{Ga} ratios.[a]

Sample	a_0 [nm]	n_{Si}/n_{Ga} gel	n_{Si}/n_{Ga} product	n_{Si}/n_{Ga} EDS	A_{BET} [$m^2 g^{-1}$]	V_p [$cm^3 g^{-1}$]	$d_{p(ads)}$, BJH [nm]	Cage diameter [nm]	Wall thickness [nm]
GaSBA-1(17)	7.77	10	16.9	16.2	1260	0.67	2.49	4.0	1.0
GaSBA-1(40)	7.89	20	39.6	40.4	1365	0.70	2.44	4.1	0.98
GaSBA-1(90)	7.83	40	90.3	93.2	1410	0.75	2.42	4.1	0.91
GaSBA-1(140)	7.77	66	139.6	135.7	1485	0.79	2.42	4.1	0.86
SBA-1	7.41	–	–	–	1150	0.60	2.20	3.7	1.06

[a] a_o = unit cell constant, A_{BET} = BET surface area, d_p = pore diameter, V_p = pore volume.

samples except GaSBA-1(17) exhibit three peaks which correspond to the (200), (210), and (211) reflections. The peaks are well resolved and can be associated with *Pm*3*n* space group, indicating that the materials are highly ordered and possess a cubic, three-dimensional, cage-type structure with open windows. GaSBA-1(17) shows three peaks at lower angle. However, the peaks are broad and are not well-resolved, indicating that the structural order of the GaSBA-1 deteriorates upon the incorporation of a larger amount of Ga in the silica framework of SBA-1. After calcination, the lower angle peaks are shifted toward higher angle with the decomposition of the organic template. Moreover, the intensity of the XRD patterns is also significantly improved after the calcination (Figure 4). This indicates that the structural

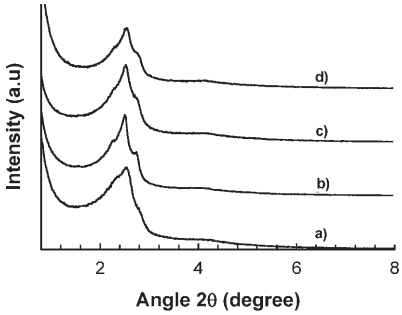

Figure 4. Powder XRD patterns of calcined GaSBA-1 materials with different Ga content: a) GaSBA-1(17), b) GaSBA-1(40), c) GaSBA-1(90), and d) GaSBA-1(140).

order is greatly improved upon calcination which is mainly due to the occurrence of the atomic arrangements in the Ga-O-Si framework of the mesoporous walls during the calcination process. In addition, the unit-cell constant of the materials, which is calculated from the formula $a_0 = d_{210}\sqrt{5}$ and is compatible with the cubic *Pm*3*n* space group, increases monotonically with decreasing the n_{Si}/n_{Ga} ratio up to 40 in the silica framework of SBA-1, and then it decreases. The unit cell constant of the materials increases from 7.77 nm for GaSBA-1(140) to 7.89 nm for GaSBA-1(40), and then decreases to 7.77 nm for GaSBA-1(17). It is also interesting to note that the wall thickness of the materials increases from 0.86 to 1.0 nm with decreasing n_{Si}/n_{Ga} ratio from 140 to 17. The increase of the unit cell constant and the wall thickness of the GaSBA-1 is directly related with the formation of more Ga-O-Si bonds in the framework, as the atomic radius of Ga^{3+} is much larger than that of the Si^{4+}, assuming that the coordination number of both the atoms is four, which leads to a longer Ga–O distance. On the other hand, the higher amount of Ga incorporation in the GaSBA-1(17) silica framework resulted in a slight reduction in the unit cell constant, revealing a partial collapse of the structural order upon Ga incorporation. From these results, it could be concluded that the Ga atoms are directly incorporated inside the framework, and the greater amount of Ga in the framework, because of its larger size, induces a small disorder in the porous structure of SBA-1.

The nitrogen adsorption–desorption isotherms of the calcined GaSBA-1 materials with different n_{Si}/n_{Ga} ratios are shown in Figure 5 and the corresponding textural properties

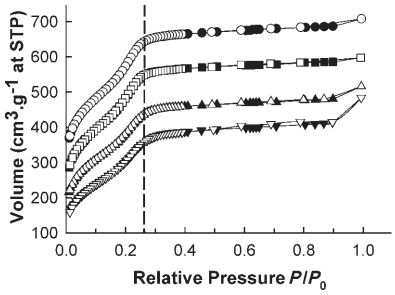

Figure 5. Nitrogen adsorption–desorption isotherms of calcined GaSBA-1 materials with different Ga content (open symbols: desorption; closed symbols: adsorption): ▼ GaSBA-1(17), ▲ GaSBA-1(40), ■ GaSBA-1(90), and ● GaSBA-1(140).

are given in Table 1. All the samples display typical type IV curve, with a sharp capillary condensation step and do not show any hysteresis loops, which is a characteristic of capillary condensation in three-dimensional materials with a small-cage-type porous structure. Moreover, the shape of the isotherm is similar to that observed for the pure silica SBA-1 materials, which posses a narrow pore structure consisting of two types of cagelike pores. It must also be noted that the capillary condensation step in the isotherms of all GaSBA-1 samples is shifted toward the higher relative pressure with increasing the Ga content, indicating that the nitrogen condensation occurs within the three-dimensional, cage-type mesopores and the samples possess better mesostructure ordering and pores are highly uniform even after the Ga incorporation. The specific surface area and specific pore volume systematically decrease with increasing the Ga content. The specific surface area amounts to 1260 m^2g^{-1} for GaSBA-1(17) and increases to 1485 m^2g^{-1} for GaSBA-1-(140), while the specific pore volume increases from 0.67 to 0.79 cm^3g^{-1}, respectively, for the same samples. The specific surface area and the specific pore volume of the GaSBA-1 samples are much higher as compared with that of pure parent silica SBA-1, indicating that the structural order of the parent SBA-1 is retained in all the GaSBA-1 samples. Analysis by the Barret–Joyner–Halenda method, which is typically used for the pore-size evaluation of mesoporous materials, reveal that all the samples possess narrow pore size distribution and the pore diameter of the materials increases with increasing Ga content (Figure 1S in the Supporting Information). However, the cage diameter of the GaSBA-1(17) sample is smaller than that of other samples, indicating the formation of small Ga_2O_3 nanoclusters in the nanocages. These results are in quite good agreement with the unit cell constant data obtained from the XRD analysis (Table 1).

The morphology of the GaSBA-1 materials with different Ga content is presented in Figure 6. A consistent increase in the size of the GSBA-1 particle with increasing the Ga content is clearly observed. In the case of GaSBA-1(90) and GaSBA-1(140), a branchlike structure composed of small spherical particles that are linked each other is clearly observed. However, an aggregate of square-shaped particles with large size is obtained for GaSBA-1(40) and (17). The large difference in the size and the shape of the particles with increasing the Ga content could be due to the presence of a large number of heteroatoms in the synthesis mixture that may disturb the condensation of metal–hydroxo species and inhibit the interaction between the gallosilicate species and the charged surfactant molecules. The interaction between the metallosilicate species and the charged surfactant molecule is very important to obtain the materials with the uniform particle size through liquid crystal (LC) assembly. The LC assembly may be affected by the large number of Ga ions in the synthesis mixture of GaSBA-1(17) and (40), which are larger in size compared to Si in the synthesis mixture, leading to particles with larger size and irregular shape.

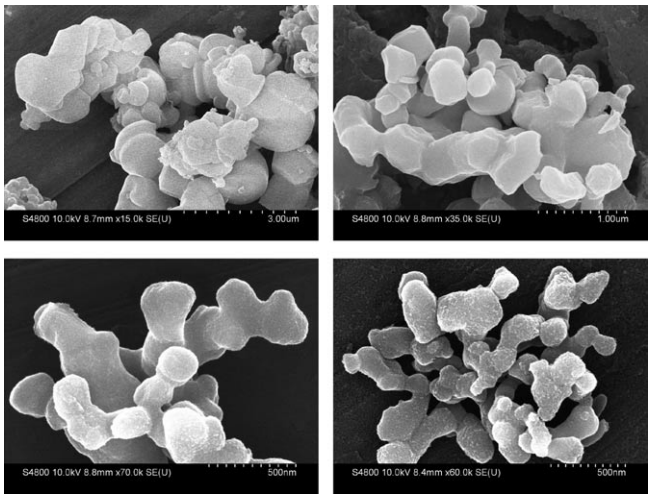

Figure 6. HRSEM images of calcined GaSBA-1 materials with different Ga content: GaSBA-1(17) (top left), GaSBA-1(40) (top right), GaSBA-1(90) (bottom left), and GaSBA-1(140) (bottom right).

To gain the better understanding of the topology of the materials after Ga incorporation, GaSBA-1 materials were characterized by HRTEM spectroscopy. Figure 7 shows the HRTEM images of the GaSBA-1(140) and GaSBA-1(17). Both the samples clearly exhibit the well-ordered porous networks, which reflect the topology of the parent SBA-1 mesoporous silica. However, a slight disorder in the porous structure was observed for GaSBA-1(17), which indicates that the structural order of the material was affected by a huge amount of Ga incorporated into the silica framework of the SBA-1 materials. These results are in quite good agreement with the data obtained from XRD and nitrogen adsorption measurements. Figure 8 shows the ^{29}Si MAS NMR spectra of GaSBA-1 samples with different n_{Si}/n_{Ga} ratios. All the samples exhibit a broad peak in the range -115 to -95 ppm. It must be noted that the sharpness of the peak decreases with increasing the Ga content in the silica matrix, presumably due to the decrease of the polymerization degree of silica with gallo hydroxo species. The peak can be deconvoluted into three peaks with the chemical shift of -110, -106, and -100 ppm. The peak centered at -110 ppm can be attributed to a Q^4 species, which represents the Si atoms bound tetragonally to four Si–O groups, whereas the peak centered at -106 ppm is attributed to Ga tetragonally bound with to three Si–O species.[39] On the other hand, the peak at -100 pm is assigned for Q^3 species, that is, Si bound to three Si–O groups and one OH group.[39] These results confirm that the Ga is indeed tetragonally incorporated with the silica framework of GaSBA-1 matrix.

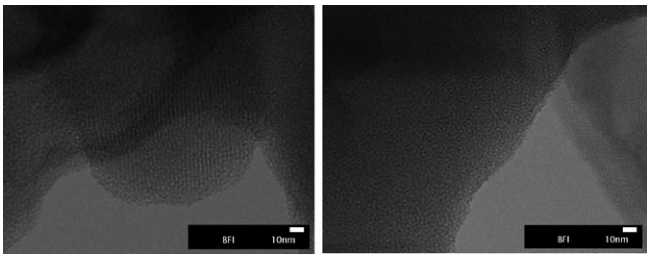

Figure 7. HRTEM images of calcined GaSBA-1(90) (left) and GaSBA-1(17) (right).

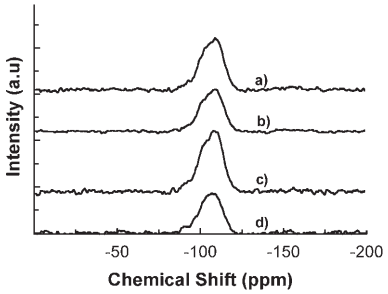

Figure 8. ^{29}Si MAS NMR spectra of calcined GaSBA-1 materials with different Ga content: a) GaSBA-1(17), b) GaSBA-1(40), c) GaSBA-1(90), and d) GaSBA-1(140).

The potential of the Ga-containing mesoporous materials for catalytic applications has been rarely reported in the literatures. Thus, special attention has been given to investigate the catalytic activity of the GaSBA-1 materials in the acid-catalyzed reaction, *tert*-butylation of phenol with *tert*-butanol (TBA) as the alkylating agent; the results are compared with the AlMCM-41 and other metal-substituted materials (Table 2). Firstly, the catalytic cycle of the GaSBA-1(17) was investigated. This was achieved by studying the *tert*-butylation of phenol in conjunction with time on stream studies over GaSBA-1(17) for a period of 6 h at 175 °C at a n_{TBA}/n_{phenol} ratio of 3 and a WHSV (weight hourly space velocity) of 5.1 h^{-1}. The products were collected once every hour. The products obtained are 2-*tert*-butylphenol (2-TBP), 4-TBP, and 2,4-di-*tert*-butylphenol (2,4-DTBP). The total conversion of phenol and the selectivity of the products as a

Table 2. Comparison of the catalytic activity of *tert*-butylation of phenol over GaSBA-1(17) with other mesoporous catalysts (reaction time: 1 h).

Reaction conditions/product details	GaSBA-1(17)	FeAlMCM-41 (20)[40]	AlMCM-41 (56)[37]	FeMCM-41 (50)[37]	FeSBA-1(36)[30]
n_{TBA}/n_{phenol}	3	3	2	2	3
WHSV [h^{-1}]	5.1	5.1	4.8	4.8	4.9
reaction temperature [°C]	175	200	175	175	200
phenol conversion [%]	84.0	70.1	35.9	21.1	78.5
selectivity [%]					
2-TBP	7.4	10.4	8.1	9.5	14.3
3-TBP	–	–	4.7	–	–
4-TBP	72.1	75.2	83.4	87	71.2
2,4-TBP	20.5	14.4	3.9	3.5	11.4

function of time are presented in Figure 9. It can be clearly seen that after one hour of reaction, which is required to achieve the stationary state, the conversion and the product

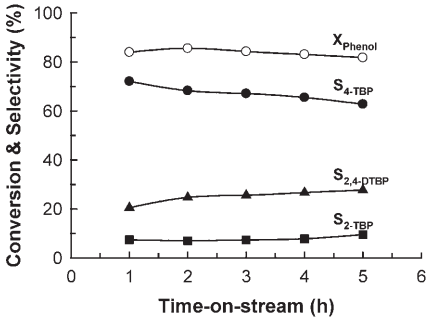

Figure 9. Effect of time on stream on the phenol conversion and the product selectivity over GaSBA-1(17) catalyst ($T_R = 175$ °C, $n_{TBA}/n_{phenol} = 3$, WHSV = 5.1 h^{-1}): ○ X_{phenol}, ● $S_{4\text{-TBP}}$, ■ $S_{2\text{-TBP}}$, and ▲ $S_{2,4\text{-DTBP}}$.

selectivities to *tert*-butylated products barely decrease over the five hour period of time-on-stream, indicating that the catalyst is highly stable and not quickly deactivated under the reaction conditions used.

The catalytic activity of *tert*-butylation of phenol as a function of Ga content for GaSBA-1 at different reaction temperatures, with a WHSV of 5.1 h^{-1} and an n_{TBA}/n_{phenol} ratio of three is shown in Figure 10. All the catalysts show a significant rise in the conversion with increasing the temperature and reaches maximum at 175 °C, and then decreases.

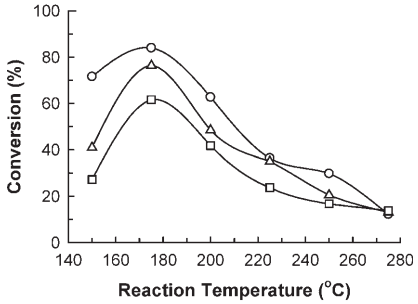

Figure 10. Effect of n_{Si}/n_{Ga} ratio and the reaction temperature on the catalytic activity of *tert*-butylation of phenol over GaSBA-1 catalysts ($n_{TBA}/n_{phenol} = 3$, WHSV = 5.1 h^{-1}): ○ GaSBA-1(17), △ GaSBA-1(40), and □ GaSBA-1(90).

Interestingly, the deactivation of the catalyst is more pronounced at temperatures higher than 200 °C, irrespective of the Ga content in the GaSBA-1 catalysts. The low conversion at high temperature may be due to the predominant dealkylation over alkylation at high temperature and also due to the diminishing availability of TBA as it undergoes side reactions, such as oligomerization or aromatization. It can also be seen in Figure 10 that the conversion of phenol decreases in the order of GaSBA-1(17) > GaSBA-1(40) > GaSBA-1(90). The catalytic activity of the same reaction over other catalysts such as FeSBA-1, FeAl-MCM-41, AlMCM-41, and FeMCM-41 are compared with that of GaSBA-1 catalysts (Table 2). Unfortunately, the GaSBA-1(90), which has the highest surface area and pore volume, was not the most active for the *tert*-butylation of phenol, probably due to the lower number of active sites on the surface of the catalyst.

It has been found that GaSBA-1(17) registered the highest phenol conversion of 84% with the selectivity to 4-TBP of 72%, which were higher than those over FeSBA-1 catalysts studied in the system. It is assumed that the higher activity of the GaSBA-1(17) is mainly due to its high acid strength, which originates from the Ga in the silica framework of SBA-1, and is known to provide acid sites with different strength. Similar results have been previously reported for Ga-substituted mesoporous materials, which show higher activity in various acid-catalyzed reactions with respect to those of other metal-substituted mesoporous materials.[32,33] On the other hand, the activity of AlMCM-41, FeMCM-41, and FeAlMCM-41 was much lower, apparently due to its unidimensional pore structure, which limits the accessibility to the acid sites, and their weaker acidity (Table 2). As the GaSBA-1(17) showed higher conversion of phenol and selectivity to 4-TBP, the catalyst was chosen for further study to investigate the effect of other reaction parameters, such as the reactant feed ratio, reaction temperature, and WHSV on the catalytic activity.

Figure 11 shows the effect of temperature on the product selectivity of *tert*-butylation of phenol over GaSBA-1(17) at a WHSV of 5.1 h^{-1} and n_{TBA}/n_{phenol} ratio of three. It is interesting to note that the selectivity to 4-TBP significantly increases with increasing the reaction temperature and reaches a maximum of 90.1% at a reaction temperature of 275 °C. Similar tendency has also been observed for FeSBA-1 catalysts.[30] The rise in the selectivity to 4-TBP with in-

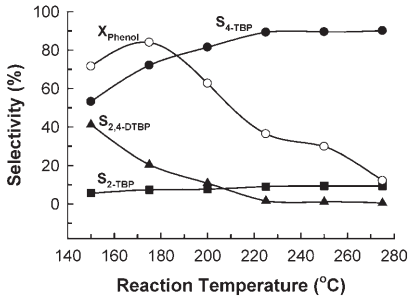

Figure 11. Effect of the reaction temperature on the conversion and the product selectivity of *tert*-butylation of phenol over GaSBA-1(17) ($n_{TBA}/n_{phenol}=3$, WHSV = 5.1 h^{-1}): ○ X_{phenol}, ● $S_{4\text{-TBP}}$, ■ $S_{2\text{-TBP}}$, and ▲ $S_{2,4\text{-DTBP}}$.

creasing the reaction temperature is likely a consequence of the easy diffusion of the 4-TBP. In addition, the above results also confirm that the formation of 4-TBP is thermodynamically favored and the higher reaction temperature does not support the secondary alkylation, which is evident from the reduction of selectivity to 2,4-DTBP at higher reaction temperature. This feature is very important from the commercial point of view, because the catalyst compensates the decrease in the conversion of phenol with increasing the reaction temperature leading to a rise in the selectivity of 4-TBP, which is commercially important product. It can also be seen from Figure 11 that the GaSBA-1(17) catalyst shows higher selectivity for 2,4-DTBP and 2-TBP at lower reaction temperatures, which decreases with a concomitant increase of the selectivity for 4-TBP, presumably due to the fact that some of the TBA molecules aew consumed through some unwanted reactions such as oligomerization and cracking.

Figure 12 shows the effect of the n_{TBA}/n_{phenol} ratio on the phenol conversion and product selectivity over the GaSBA-1(17) catalyst at the reaction temperature of 175 °C and WHSV of 5.1 h^{-1}. Increasing the n_{TBA}/n_{phenol} ratio from 1 to 3 resulted in an increase in the conversion of phenol from 44 % to 84.0 %. The increase in phenol conversion with increasing n_{TBA}/n_{phenol} ratio may be attributed to a competition between the polar molecule TBA and phenol for adsorption sites. However, with a further increase of the n_{TBA}/n_{phenol} ratio to 4 had a negative role on the conversion of phenol, which significantly decreases. This could be mainly due to

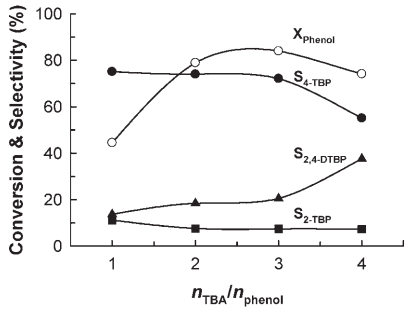

Figure 12. Effect of n_{TBA}/n_{phenol} on the conversion and the product selectivity of *tert*-butylation of phenol over GaSBA-1(17) ($T_R = 175$ °C, WHSV = 5.1 h^{-1}): ○ X_{phenol}, ● $S_{4\text{-TBP}}$, ■ $S_{2\text{-TBP}}$, and ▲ $S_{2,4\text{-DTBP}}$.

the blocking of active sites by the adsorption of either the excess of TBA or the water molecules produced from the dehydration of alcohol. As expected, the selectivity to 4-TBP decreases with the concomitant increase of 2,4-DTBP with increasing the concentration of TBA molecules in the reaction feed, most probably due to the availability of excess of the alkylating agent.

An increase in the WHSV of the feed from 1.7 to 5.1 h^{-1} leads to an increase in the conversion of phenol from 74.1 to 84 % (Figure 13). However, a reduction in the phenol conversion is observed when the WHSV is increased from 5.1 to 6.8 h^{-1}, most likely due to the shorter contact time at higher space velocity. Interestingly, the selectivity to 4-TBP increases from 66.3 to 73 % with increasing the WHSV from 1.7 to 6.8 h^{-1}, whereas the selectivity to 2,4-DTBP significantly decreases when the WHSV of the reactant feed is increased, which is mainly due to the longer contact time that stimulates the cracking reaction at the catalyst surface and diminish the availability of the *tert*-butyl cation at lower WHSV. These results indicate that the higher selectivity to 2,4-DTBP requires a low WHSV of reactant feed or a large contact time between the catalyst surface and the feed, whereas the higher WHSV facilitates the formation of monoalkylated products, which is mainly due to the less contact time between the alkylating agent and the actives sites present in the surface of the GaSBA-1(17) catalyst.

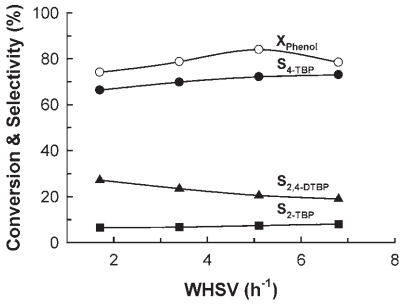

Figure 13. Effect of WHSV on the conversion and the product selectivity of *tert*-butylation of phenol over GaSBA-1(17) ($T_R = 175$ °C, $n_{TBA}/n_{phenol} = 3$): ○ X_{phenol}, ● $S_{4\text{-TBP}}$, ■ $S_{2\text{-TBP}}$, and ▲ $S_{2,4\text{-DTBP}}$.

Conclusion

We strikingly demonstrate for the first time the successful preparation of novel three-dimensional gallosilicate materials (GaSBA-1) with a well-ordered, cage-type porous structure and excellent textural parameters through an organic self-assembly process with a cationic surfactant in a highly acidic medium. XRD and nitrogen adsorption results revealed that the three-dimensional, cage-type pore structure with open windows is retained in the GaSBA-1 even after a large amount of Ga is incorporated into the silica framework. Interestingly, the specific surface area and the specific pore volume of the GaSBA-1 materials are significantly in-

creased after Ga incorporation; these factors are very important and determine the catalytic activity of the materials. Moreover, it has been demonstrated that particle morphology and the pore diameter of the materials can be controlled by incorporating Ga atoms in the silica framework of SBA-1 matrix. Finally, the catalytic activity in the *tert*-butylation of phenol with *tert*-butanol as the alkylating agent has been investigated and the catalysts showed a remarkable activity, with very high substrate conversion and the selectivity to 4-*tert*-butylated phenol product. Moreover, the GaSBA-1 catalysts are found to be superior over other catalysts such as AlMCM-41, FeSBA-1, FeAl-MCM-41, and FeMCM-41 in the above-mentioned reaction. Thus, we strongly believe that the novel highly active GaSBA-1 catalysts could be utilized for many acid-catalyzed organic transformations, and offer an economic and environmentally friendly way for the production of variety of fine chemical synthesis, as supports for sensing, and in adsorption processes.

Experimental Section

Materials: Cetyltriethylammonium bromide (CTEABr) was used as the structure-directing reagent. Tetraethyl orthosilicate (TEOS; Aldrich) and Ga nitrate (Wako) were used as the sources for Si and Ga, respectively. Phenol, TBA, *tert*-butylphenols, and hydrochloric acid (36wt%) were obtained from Wako chemicals and used as received without further purification.

Synthesis of the surfactant: The surfactant (CTEABr) was synthesized by reaction of 1-bromohexadecane with an equimolar amount of triethylamine in ethanol under reflux conditions for two days. A typical synthesis procedure for CTEABr is as follows: 1-bromohexadecane (31.5 g) was dissolved in absolute ethanol (197.25 g). Subsequently, triethylamine (10.2 g) was added to the reaction mixture. The resultant mixture was heated while being stirred for 48 h under reflux conditions. The solvent was evaporated on a rotary evaporator until a white viscous liquid was obtained, and then placed in a water bath to get a solid white product. The brown liquid turned to a solid upon cooling to room temperature. The resulting solid CTEABr was purified by recrystallization from a chloroform/ethyl acetate mixture. The mixture was cooled in a refrigerator in order to increase precipitation. The resultant precipitate was filtered, washed with ethyl acetate, and dried in a vacuum oven at room temperature.

Synthesis of Ga-containing SBA-1: Ga-containing SBA-1 was synthesized under acidic conditions by using CTEABr as the surfactant, TEOS as the silica source and gallium nitrate as the Ga source. A typical synthesis procedure for GaSBA-1 is as follows: CTEABr (2.44 g) was added to HCl (78.44 mL, 3.82 M). The solution thus obtained was cooled to 0 °C and stirred for 30 min under cold condition. Then, TEOS (6.25 g) which was precooled to 0 °C and an appropriate quantity of Ga nitrate were added to the solution under vigorous stirring. The stirring was continued for another 5 h at 0 °C. Thereafter, the reaction mixture was heated to 100 °C for 1 h. The solid products were recovered by filtration and dried in an oven at 100 °C overnight. The samples were labeled GaSBA-1(x), in which x denotes the n_{Si}/n_{Ga} molar ratio in the final product. The molar composition of the initial synthesis gel was 1 TEOS:0.0075–0.05 Ga_2O_3:0.2 CTEABr:10 HCl:125 H_2O. The as-synthesized materials were then calcined in air by raising the temperature from 20 to 550 °C with a heating rate of 1.8 °C min^{-1} and keeping the sample at the final temperature for 10 h in oxygen.

Physical measurements: The powder X-ray diffraction patterns of GaSBA-1 materials were collected on a Siemens D5005 diffractometer by using $Cu_{K\alpha}$ ($\lambda = 0.154$ nm) radiation. The diffractograms were recorded in the 2θ range of 0.8 to 10° with a 2θ step size of 0.01° and a step time of 10 s. Nitrogen adsorption and desorption isotherms were measured at −196 °C on a Quantachrome Autosorb 1 sorption analyzer. All samples were outgassed for 3 h at 250 °C under vacuum ($p < 10^{-5}$ hPa) in the degas port of the adsorption analyzer. The specific surface area was calculated by using the BET model. The pore size distributions were obtained from the adsorption branch of the nitrogen isotherms by using the corrected form of the Kelvin equation by means of the Barrett–Joyner–Halenda method as proposed by Kruk et al. [Eq. (1)][38]

$$r(p/p_0) = 2\gamma V_L/RT\ln[p_0/p] + t(p/p_0) + 0.3\ \text{nm} \quad (1)$$

In Equation (1), V_L is the molar volume of the liquid adsorbate, γ is its surface tension (8.88×10^{-3} N m^{-1}), R is the gas constant (8.314 J mol^{-1} K^{-1}), T is the absolute temperature (77 K), and $t(p/p_0)$ is the statistical film thickness of nitrogen adsorbate in pores of the SBA-1 as a function of the relative pressure p/p_0.

Elementary analysis was done by using an Analyst AA 300 spectrometer. The HRTEM images were obtained with JEOL JEM-2100F. The preparation of samples for HRTEM analysis involved sonication in ethanol for 5 min and deposition on a copper grid. The accelerating voltage of the electron beam was 200 kV. The morphology of the materials was obtained with Hitachi S-4800 HR-FESEM by using an acceleration voltage of 10 kV, whereas the elemental mapping and EDS analysis of the samples were obtained on the above instrument by using an acceleration voltage of 20 kV. The ^{29}Si MAS NMR spectra were recorded at a resonance frequency of 99.361 MHz at a Bruker MSL 500 spectrometer, employing a 7 mm zirconia rotor with a spinning frequency of 4.5 kHz, a pulse length of 3 μs, delay time of 30 s, and between 1500 to 3000 scans were accumulated to obtain a good signal to noise ratio. All spectra were referenced against external tetramethylsilane (0 ppm).

Catalytic investigations: The *tert*-butylation of phenol was carried out in a fixed-bed down flow-type reactor made up of a borosil glass tube with a length of 40 cm and an internal diameter of 2 cm. About 0.5 g of catalyst was placed in the reactor and supported on either side with a thin layer of quartz wool and ceramic beds. The reactor was heated to the reaction temperature with the help of a tubular furnace controlled by a digital temperature controller. The catalyst was activated in air at 550 °C for 6 h prior to the catalytic runs. Reactants were fed into the reactor by using a syringe infusion pump. The bottom of the reactor was connected to a coiled condenser and receiver to collect the products. The products obtained in the first 20 minutes were discarded and the product collected after one hour was analyzed for identification. The liquid products were analyzed on a Shimadzu gas chromatograph GC-17 A by using a DB-5 capillary column. Product identification was achieved by co-injection and GC-MS.

Acknowledgement

This work was financially supported by Japan Science and Technology under the Strategic Program for Building an Asian Science and Technology Community Scheme.

[1] J. S. Beck, J. C. Vartuli, W. J. Roth, M. E. Leonowicz, C. T. Kresge, K. D. Schmitt, C. T.-W. Che, D. H. Olson, E. W. Sheppard, S. B. McCullen, J. B. Higgins, J. L. Schlenker, *J. Am. Chem. Soc.* **1992**, *114*, 10834.
[2] C. T. Kresge, M. E. Leonowicz, W. J. Roth, J. C. Vartuli, J. S. Beck, *Nature* **1992**, *359*, 710.
[3] D. Zhao, Q. Huo, J. Feng, B. F. Chmelka, G. D. Stucky, *J. Am. Chem. Soc.* **1998**, *120*, 6024.
[4] Q. Huo, D. I. Margolese, G. D. Stucky, *Chem. Mater.* **1996**, *8*, 1147.
[5] P. Yang, D. Zhao, D. Margolese, B. F. Chmelka, G. D. Stucky, *Nature* **1998**, *396* 152.

[6] P. Yang, D. Zhao, D. Margolese, B. F. Chmelka, G. D. Stucky, *Chem. Mater.* **1999**, *11*, 2831.
[7] J. F. Diaz, K. J. Balkus, *J. Mol. Catal. B* **1996**, *2*, 115.
[8] Z. Luan, H. He, W. Zhou, C.-F. Cheng, J. Klinowski, *J. Chem. Soc. Faraday Trans.* **1995**, *91*, 2955.
[9] Z. Luan, C.-F. Cheng, H. He, J. Klinowski, *J. Phys. Chem.* **1995**, *99*, 10590.
[10] Y. Yue, A. Gédéon, J.-L. Bonardet, N. Melosh, J.-B. D'Espinose, J. Fraissard, *Chem. Commun.* **1999**, 1967.
[11] Z. Luan, M. Hartmann, D. Zhao, W. Zhou, L. Kevan, *Chem. Mater.* **1999**, *11*, 1621.
[12] M. Hartmann, A. Vinu, Langmuir **2002**, *18*, 8010.
[13] A. Vinu, V. Murugesan, M. Hartmann, *J. Phys. Chem. B* **2004**, *108*, 7323.
[14] A. Vinu, V. Murugesan, O. Tangermann, M. Hartmann, *Chem. Mater.* **2004**, *16*, 3056.
[15] A. Vinu, V. Murugesan, W. Böhlmann, M. Hartmann, *J. Phys. Chem. B.* **2004**, *108*, 11496.
[16] S. Che, A. E. G. Bennet, Y. Yokoi, K. Sakamoto, H. Kunieda, O. Terasaki, T. Tatsumi, *Nat. Mater.* **2003**, *2*, 801.
[17] Q. Zhang, K. Ariga, A. Okabe, T. Aida, *J. Am. Chem. Soc.* **2004**, *126*, 988.
[18] Q. Huo, R. Leon, P. M. Petroff, G. D. Stucky, *Science* **1995**, *268*, 1324.
[19] P. T. Tanev, T. J. Pinnavaia, *Science* **1995**, *267*, 865.
[20] S. A. Bagshaw, E. Prouzet, T. J. Pinnavaia, Science **1995**, *269*, 1242.
[21] A. Vinu, T. Krithiga, V. Murugesan, M. Hartmann, *Adv. Mater.* **2004**, *16*, 1817.
[22] C. Zapilko, R. Anwander, *Chem. Mater.* **2006**, *18*, 1479.
[23] A. E. Garcia-Bennett, S. Williamson, P. A. Wright, I. J. Shannon, *J. Mater. Chem.* **2002**, *12*, 3533.
[24] M. Kruk, M. Jaroniec, R. Ryoo, J. M. Kim, *Chem. Mater.* **1999**, *11*, 2568.
[25] S. Che, Y. Sakamoto, O. Terasaki, T. Tatsumi, *Chem. Mater.* **2001**, *13*, 2237.
[26] A. Vinu, V. Murugesan, M. Hartmann, *Chem. Mater.* **2003**, *15*, 1385.
[27] L.-X. Dai, K. Tabata, E. Suzuki, T. Tatsumi, *Chem. Mater.* **2001**, *13*, 208.
[28] L.-X. Dai, Y.-H. Teng, K. Tabata, ; E. E. Suzuki, T. Tatsumi, *Chem. Lett.* **2000**, 794; E. E. Suzuki, T. Tatsumi, *Chem. Lett.* **2000**, 794.
[29] S. Che, Y. Sakamoto, O. Terasaki, T. Tatsumi, *Chem. Mater.* **2001**, *13*, 2237.
[30] a) A. Vinu, J. Dedecek, V. Murugesan, M. Hartmann, *Chem. Mater.* **2002**, *14*, 2433; b) M. Hartmann, A. Vinu, S. P. Elangovan, V. Murugesan, W. Böhlmann, *Chem. Commun.* **2002**, *11*, 1238; c) A. Vinu, T. Krithiga, V. V. Balasubramanian, A. Asthana, P. Srinivasu, T. Mori, K. Ariga, G. Ramanath, P. G. Ganesan, *J. Phys. Chem. B* **2006**, *110*, 11924.
[31] a) A. Vinu, P. Srinivasu, D. P. Sawant, S. Alam, T. Mori, K. Ariga, V. V. Balasubramanian, C. Anand, *Microporous Mesoporous Mater.* **2008**, *110*, 422; b) A. Vinu, T. Krithiga, N. Gokulakrishnan, P. Srinivasu, S. Anandan, K. Ariga, V. Murugesan, V. V. Balasubramanian, T. Mori, *Microporous Mesoporous Mater.* **2007**, *100*, 87.
[32] H. Kosslick, G. Lischke, B. Parlitz, W. Storek, R. Frike, *Appl. Catal. A* **1999**, *184*, 49.
[33] R. Birjega, C. Nenu, R. Ganea, Gr. Pop, S. Serban, T. Blasco, *Stud. Surf. Sci. Catal.* **2002**, *142*, 1331.
[34] A. Knop, L. A. Pilato, *Phenolic Resin Chemistry*, Springer, Berlin, **1985**.
[35] a) J. B. Niederl, S. Natelson, *J. Am. Chem. Soc.* **1931**, *53*, 272; b) K. G. Chandra, M. M. Sharma, *Catal. Lett.* **1993**, *19*, 309.
[36] K. Zhang, C. Huang, H. Zhang, S. Xiang, S. Liu, D. Xu, H. Li, *Appl. Catal. A* **1998**, *166*, 89.
[37] a) A. Sakthivel, S. K Badamali, P. Selvam, *Microporous Mesoporous Mater.* **2000**, *39*, 457; b) S. K. Badamali, A. Sakthivel, P. Selvam, *Catal. Lett.* **2000**, *65*, 153; c) A. Sakthivel, N. Saritha, P. Selvam, *Catal. Lett.* **2001**, *72*, 225.
[38] M. Kruk,, M. Jaroniec, A. Sayari, *Langmuir* **1997**, *13*, 6267.
[39] C.-F. Cheng, H. He, W. Zhou, J. Klinowski, J. A. S. Goncalves, L. F. Gladden, *J. Phys. Chem.* **1996**, *100*, 390.
[40] A. Vinu, K. Usha Nandhini, V. Murugesan, V. Umamaheswari, A. Pöppl, M. Hartmann, *Appl. Catal. A* **2004**, *265*, 1.

Received: December 8, 2007
Published online: March 11, 2008

